

# Free log-likelihood as an unbiased metric for coherent diffraction imaging

Vincent Favre-Nicolin

*ESRF, The European Synchrotron, 71 Avenue des Martyrs, 38000 Grenoble, France and  
Univ. Grenoble Alpes, Grenoble, France\**

Steven Leake and Yuriy Chushkin

*ESRF, The European Synchrotron, 71 Avenue des Martyrs, 38000 Grenoble, France*

(Dated: December 20, 2024)

Coherent Diffraction Imaging (CDI), a technique where an object is reconstructed from a single (2D or 3D) diffraction pattern, recovers the lost diffraction phases without *a priori* knowledge of the extent (support) of the object, which prevents an unambiguous metric evaluation of solutions. We propose to use a 'free' log-likelihood indicator, where a small percentage of points are masked from the reconstruction algorithms, as an unbiased metric to evaluate the validity of proposed solutions, independent of the sample studied. We also show how a set of solutions can be analysed through an orthonormal decomposition to yield a better estimate of the real object.

PACS numbers: 87.59.-e, 41.50.+h, 42.25.Kb

## I INTRODUCTION

Coherent Diffraction Imaging (CDI) is a technique which exploits the coherence properties of a light source, here synchrotron generated X-ray beams [1–5] are employed to reconstruct isolated two or three-dimensional objects from their diffraction pattern alone - an approach which can also be used with soft X-ray sources [6] and coherent electron beams [7, 8]. This can also be applied in the Bragg geometry to yield quantitative strain information [9–13]. CDI has been successfully used on a wide range of samples, from single cells [14] to inorganic particles [15, 16], with applications exploiting the temporal properties of X-ray Free Electron Lasers to viruses [17] and time-resolved strain analysis [18].

As CDI is based on the measurement of the far-field diffraction pattern of a single object, the reconstruction is only possible if the diffraction pattern is recorded at a spacing finer than the Nyquist frequency (this condition is called *oversampling*) [1, 3, 19]. This is easily done experimentally if the sample size can be estimated, and a variety of algorithms such as Error Reduction (ER), Hybrid Input-Output (HIO), Relaxed Averaged Alternating Reflectors (RAAR), Charge Flipping (CF), etc... can be used to phase the diffraction pattern and reconstruct the object [5, 20, 21].

However the weakness of CDI lies in the absence of reliable figures of merit to assess the quality of the reconstructed objects. In principle, it is easy to define a figure of merit by comparing the observed diffraction pattern to the calculated one. But as the diffraction pattern is oversampled and the actual size and shape of the object is *a priori* unknown, it is easy to create incorrect solutions which involve an object size larger than the real one (i.e. with many extra free parameters), and thus yield a better figure of merit.

In this article, we propose a free log-likelihood as an

objective figure of merit that outperforms the available ones. Then we show how it can be applied to evaluate the solutions and combine them in the final optimal reconstruction.

## II FIGURES OF MERIT

A number of figures of merit have been proposed, working either in the object or Fourier-space domain. A list of the most used figures of merit is shown in table I. Note that the most quantitative approach to a reliable figure of merit was proposed for Ptychography [22], using a likelihood based analysis which considers e.g. Poisson noise.

In order to evaluate how discriminating these figures are, we used an 2D diffraction dataset, from an ESRF logo sample, recorded at the ID10 beamline [15] (see [24] for experimental details). In Fig.1 the diffraction data and several reconstructed solutions are shown, which have been obtained by starting from a random object, with 400 Hybrid Input-Output cycles followed by 200 Error Reduction cycles, using a fixed support<sup>1</sup>. The three solutions were generated using either (b) a tight support (4353 pixels), (c) a tight support radially expanded by two pixels, or (d) a large support (tight +7 pixels). As is clearly seen in Fig. 1, the best result is obtained by a tight support, and quickly degrades for larger supports. As can be seen in table I, none of the proposed figures of merit are discriminating: while the solution in Fig. 1a) obtained from a tight support is obviously the best and

<sup>1</sup> Note that the actual algorithm used here is irrelevant, as any global optimisation scheme will produce a distribution of solutions, and the aim of this article is to provide a way to assess their quality. We deliberately did not impose positivity to have a large enough range of solutions to evaluate.

Figure of merit	tight (1b)	+2 pixels (1c)	large (1d)	eigen-10 (3a)	average-10 (3b)	eigen-4
$nb_{support}$	4353	10460	17616	-	-	-
$E_o^2 = \sum_{i \notin \Omega}  \rho_i ^2 / \sum_i  \rho_i ^2$	4.9e-3	3.3e-3	4.5e-3	1.4e-2	3e-2	6e-3
$E_F^2 = \sum  F_i^{calc} - F_i^{obs} ^2 / \sum  F_i^{obs} ^2$	0.8559	0.8557	0.8558	0.8590	0.8610	0.8570
$LLK = -\frac{1}{N} \sum_i \log \frac{(I_i^{calc})^{I_i^{obs}}}{I_i^{obs!}} e^{-I_i^{calc}}$	68	46	45	100	148	82
$LLK_{free}$	83	122	323	98	149	80

TABLE I. Figures of merit for CDI analysis:  $E_o^2$  is the object-domain error [4, 21], where  $\Omega$  denotes the object support (i.e. the area or volume where the object lies), and  $\rho_i$  is the density inside the object.  $E_F^2$  is the Fourier-space domain error [4, 21, 23] comparing calculated and observed amplitudes (this formula can also be used based on intensities).  $LLK$  is the Poisson log-likelihood[22], where  $I_i^{obs}$  and  $I_i^{calc}$  are, respectively, the observed and calculated intensity at pixel  $i$  of the diffraction data.  $LLK_{free}$  is the Poisson log-likelihood computed only over a 'free' set of pixels (see section III). The figures correspond either to the three solutions shown in Fig.1, or to the eigen- and average solutions discussed in section IV and shown in Fig.3. Only the  $LLK_{free}$  allows to correctly discriminate between individual reconstructions.

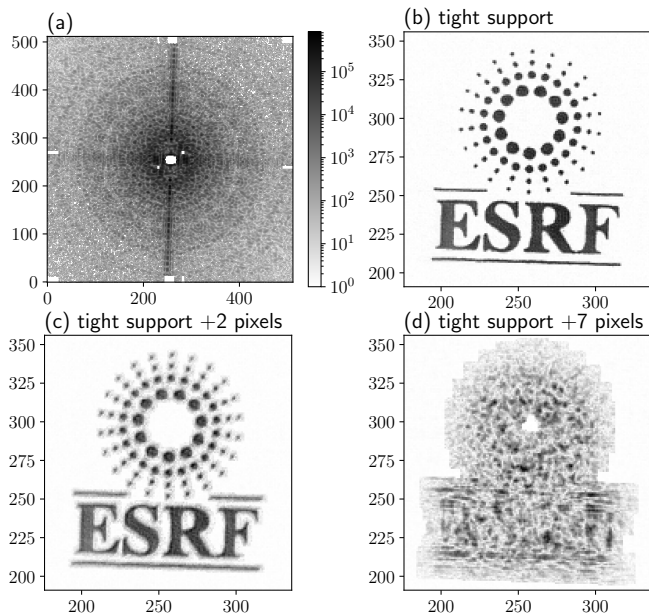


FIG. 1. (a) Coherent X-ray diffraction pattern of the ESRF logo. Examples of the reconstructed logo obtained using (b) a tight support, (c) a tight support expanded by two pixels (producing more noise around the object), and (d) a large support. For each reconstruction, the average Poisson log-likelihood is reported, as well as the free log-likelihood - the former does not allow to discriminate solutions, and allows clearly diminished results like (d) to have lower log-likelihood, whereas the free log-likelihood clearly discriminates them.

corresponds to the scanned sample [24], both the object-domain error and the Fourier-based metric  $E_F^2$  shows little difference between the solutions, and are higher for the correct tight support solution. This is clearer for the  $LLK$ , which is worse for the tight solution (b) even though it is the best result. The main reason for these conflicting results is that the more points there are in the support, the more free parameters the algorithm can use to better fit the diffraction data - Fig. 1d) shows a clear case of over-fitting.

From this example one concludes that it is essential to simultaneously achieve both: a good fit between the calculated and observed diffraction pattern, and a tight support around the object. This has long been known and efficient algorithms, such as the shrink-wrap approach [5], exist to produce a tight support, which will normally yield a unique solution in two or three dimensions [25–30].

Other constraints or figures of merit can be used based on physical properties, but they rely strongly on *a priori* knowledge of the object and thus are limited in application. For example, positivity of the reconstructed object (e.g. when operating in the small-angle regime for a thin object, or in the Bragg regime for an unstrained nanocrystal), or enforcing phase, density or other *ad hoc* constraints[31].

The lack of an unambiguous evaluation metric often leads to the need to visually inspect, evaluate and select solutions, which is very slow, and hence unpractical. As brighter X-ray sources pave the way for serial CDI experiments with larger data throughput [32, 33], the need, for a discriminating figure of merit to sort the proposed solutions without requiring a visual inspection, is paramount.

### III FREE LOG-LIKELIHOOD

The risk of misleading figures of merit due to over-fitting also exists e.g. in macro-molecular crystallography, where the large number of parameters (the atomic positions) must be refined against the available diffraction data: in order to avoid over-fitting, it was proposed[34–36] to measure a free R-factor, which would set aside a small percentage of diffraction data (the 'free' set) and refine the structure against the remaining 'working set' of data. The  $R_{free}$  is then evaluated only by comparing the calculated diffraction data against the 'free' set, producing an un-biased figure of merit. This approach is more generally known as jack-knifing [37, 38], and was developed for unbiased statistical evaluation.

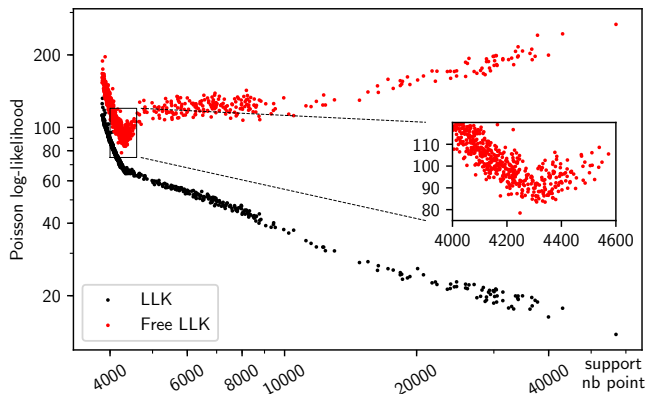


FIG. 2. Scatter plot of log-likelihood (black) and free log-likelihood (red) vs the number of points in the support, obtained by generating 1000 solutions with random starting objects and different parameters. While the overall log-likelihood decreases with the number of points in the final support, the free log-likelihood points to an optimal support size around 4300 points.

This approach is even more appealing for CDI because of the large uncertainty of the support area (contrary to refinement in crystallography where the atomic sequence or chemical formula is usually known). We have implemented this in the PyNX accelerated coherent imaging toolkit [39], which can be used for CDI analysis:

- $\approx 5\%$  of the observed diffraction data is set aside in a 'free' set of pixels with pixels, which are grouped as islands of radius 3 pixels - to make sure that correlations between neighbouring pixels (a by-product of oversampling) does not create a strong relationship between the working set and the 'free' set.
- The free pixels are randomly located in the dataset, only excluding the center of the diffraction pattern (5% of the maximum radius): this area can include a large number of photons, and masking those can hinder the initial estimate of the object.
- when performing the usual projection algorithms [20], in the Fourier update step (replacing the calculated amplitudes with the observed ones while keeping the calculated phases), pixels in the 'free' set are considered masked and keep their calculated complex amplitude.

In the following we will only report the free Poisson log-likelihood  $LLK_{free}$  figure of merit, because the photon counting properties of modern X-ray detectors theoretically make Poisson log-likelihood the natural choice. However, we would like to point out that the ensuing discussion and examples would be identical with any other noise model or Fourier based metric.

As is shown in Table. I, the free log-likelihood correctly discriminates between the three proposed solutions (tight support, +2 pixels, +7 pixels).

We conducted a more systematic study using the same dataset and performed 1000 optimisations using a similar approach: starting from a random object with an initial tight support expanded by a radius of 7 pixels, then performing 400 HIO cycles followed by 200 ER cycles, updating the support every 20 cycles, with a support threshold[5] randomly chosen between 0.25 to 0.4<sup>2</sup>. Both  $LLK$  and  $LLK_{free}$  are plotted against the final number of pixels in the support for all solutions in Fig. 2. In this graph the normal  $LLK$  (measured against the 'working' set) monotonically decreases as the number of points in the support increases, even if an inflection point is clearly visible.  $LLK_{free}$  however, displays a clear minimum around 4300 pixels, which corresponds to an optimal solution similar to that in Fig. 1b.

While this demonstrates the capability of  $LLK_{free}$  to serve as an unbiased figure of merit, we should point out two limitations: firstly, there is nothing preventing an incorrect model to have a low  $LLK_{free}$  by chance - however as is shown in Fig. 2 with 1000 generated solutions, it is statistically improbable. Secondly,  $LLK_{free}$  is not an *absolute* figure of merit, and a single value cannot indicate the validity of the solution. Generating a number of solutions and to combining them in an optimal manner remains a necessity.

#### IV EIGEN- AND AVERAGE SOLUTIONS

Once a set of solutions has been produced, usually a selection of the best solutions are averaged and then compared against the diffraction data, e.g. by plotting the Phase Retrieval Transfer Function (PRTF)[14, 15, 23], which is the ratio of the average calculated amplitude to the observed amplitude, as a function of the resolution ring (a fraction of the sampling frequency of the dataset). The relative frequency at which the PRTF falls below 50% can be used as an indication of the cross-correlation between the chosen solutions, and of the resolution of the reconstruction.

An alternative approach to averaging consists in computing eigenvectors for the selected solutions, which yields a set of orthonormal 'eigen-solutions' (as many as combined), as shown in Fig. 3. This method presents a few advantages compared to averaging: firstly, it is less sensitive to outlier solutions than averaging (a single outlier would contribute to secondary modes in the

<sup>2</sup> Note that we did not impose positivity: that and the random threshold values leads to a wide range of solutions for statistical purposes. With a positivity constraint, most solutions would have been much closer to the optimal one

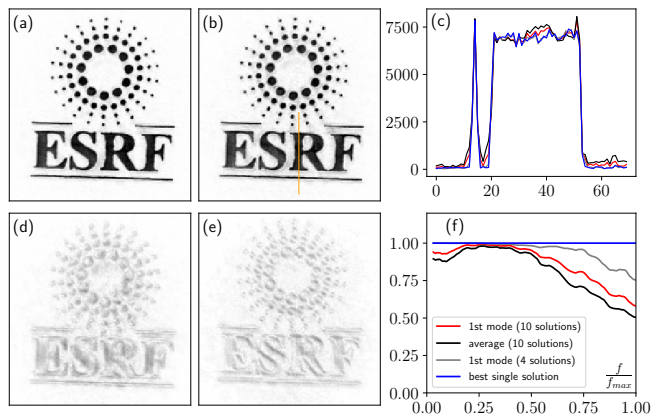


FIG. 3. Combination of ten solutions: (a) the first eigen-solution obtained by computing an eigenvalue decomposition (76% weight), (b) average of the solutions (c) line cut (indicated in orange in (b)), with the first eigen-solution in red, the average solution in black, the best individual solution in blue, and in gray the first eigen-solution when combining only the 4 best solutions (weighting 99% of the 4 solutions). (d) 2<sup>nd</sup> and (e) 3<sup>rd</sup> eigen-solutions in the ten mode decomposition. (f) phase retrieval transfer function computed for the different types of solutions. The solution obtained through eigen-decomposition of the 10 solutions yields a higher correlation at high frequencies, and presents lower background noise levels compared to the average solution. Combining only the 4 best solutions yields a higher PRTF.

eigenvector decomposition), and secondly, it also yields a weight (its overall squared amplitude) for each eigen-solution, which can be also used as an indicator of the cross-correlation between solutions, ideally the relative weight of the first (strongest) eigen-solution should be as close to 100% as possible.

Fig. 3 shows the result of combining either the 10 or 4 best (lowest  $LLK_{free}$ ) solutions<sup>3</sup> from 50 optimisations, obtained with the same procedure as those in Fig.2, and after subpixel alignment[40] and phase matching of the solutions.

The most intense mode (Fig. 3a) represents 76% of the 10 solutions, and is similar to the average (Fig. 3b) but with slightly reduced background noise outside the main object (also see the line cut in Fig.3c). The secondary modes (e.g. Fig. 3d) and e)) can be used as an indicator of where the proposed solutions have more diversity. The PRTF (Fig. 3f)) shows that the first decomposed mode yields a higher resolution than the average solution, but remains inferior to the first mode of only

<sup>3</sup> The 10 best selected solutions had up to 16300 points in the support and a  $LLK_{free}$  up to 255, while the 4 best had up to 5100 points with a  $LLK_{free}$  lower than 148. The purpose of keeping all 10 solutions is to evaluate the efficiency of combining imperfect solutions, which is often the case in CDI. The shown figures were tested against several generated set of solutions with similar results.

the 4 best solutions (this mode then represents 99% of the selected 4). Note that when only a subset of close-to-optimal solutions are selected, there is little difference between the first mode and the average (identical PRTF).

## V CONCLUSION

In this article we have shown that using a free log-likelihood figure-of-merit allows one to evaluate solutions from CDI optimisations in a unbiased manner, despite the lack of *a priori* knowledge of the object support size and shape. Moreover using an orthonormal mode decomposition of the best solutions yields a better solution less prone to outlier results compared to the usual averaging approach.

The main advantage of this method is that it is completely generic, as it does not rely on any *a priori* knowledge on the sample (complex-valued or real-valued object, homogeneity of density or phase, etc...), and can thus be used for *unsupervised* phasing. This method should be particularly relevant for high data throughput approaches which are now being developed with X-ray free electron laser and brighter synchrotron sources.

The authors would like to acknowledge Federico Zontone for the help with the CDI measurements.

\* favre@esrf.fr

- [1] D. Sayre, H. N. Chapman, and J. Miao, Acta Crystallographica Section A: Foundations of Crystallography **54**, 232 (1998).
- [2] J. Miao, P. Charalambous, J. Kirz, and D. Sayre, Nature **400**, 342 (1999).
- [3] J. Miao and D. Sayre, Acta Crystallographica Section A Foundations of Crystallography **56**, 596 (2000).
- [4] J. Miao, K. O. Hodgson, and D. Sayre, PNAS **98**, 6641 (2001).
- [5] S. Marchesini, H. He, H. N. Chapman, S. P. Hau-Riege, A. Noy, M. R. Howells, U. Weierstall, and J. C. H. Spence, Phys. Rev. B **68**, 140101 (2003).
- [6] R. L. Sandberg, A. Paul, D. A. Raymondson, S. Hädrich, D. M. Gaudiosi, J. Holtsnider, R. I. Tobey, O. Cohen, M. M. Murnane, H. C. Kapteyn, C. Song, J. Miao, Y. Liu, and F. Salmassi, Physical Review Letters **99**, 098103 (2007).
- [7] J. M. Zuo, I. Vartanyants, M. Gao, R. Zhang, and L. A. Nagahara, Science **300**, 1419 (2003).
- [8] W. J. Huang, R. Sun, J. Tao, L. D. Menard, R. G. Nuzzo, and J. M. Zuo, Nat Mater **7**, 308 (2008).
- [9] I. K. Robinson, I. A. Vartanyants, G. J. Williams, M. A. Pfeifer, and J. A. Pitney, Phys. Rev. Lett. **87**, 195505 (2001).
- [10] G. J. Williams, M. A. Pfeifer, I. A. Vartanyants, and I. K. Robinson, Phys. Rev. Lett. **90**, 175501 (2003).
- [11] M. A. Pfeifer, G. J. Williams, I. A. Vartanyants, R. Harder, and I. K. Robinson, Nature **442**, 63 (2006).
- [12] V. Favre-Nicolin, F. Mastropietro, J. Eymery, D. Cama-

- cho, Y. M. Niquet, B. M. Borg, M. E. Messing, L.-E. Wernersson, R. E. Algra, E. P. A. M. Bakkers, T. H. Metzger, R. Harder, and I. K. Robinson, *New J. Phys.* **12**, 035013 (2010).
- [13] I. Robinson and R. Harder, *Nat Mater* **8**, 291 (2009).
- [14] D. Shapiro, P. Thibault, T. Beetz, V. Elser, M. Howells, C. Jacobsen, J. Kirz, E. Lima, H. Miao, A. M. Neiman, and D. Sayre, *PNAS* **102**, 15343 (2005).
- [15] Y. Chushkin, F. Zontone, E. Lima, L. De Caro, P. Guardia, L. Manna, and C. Giannini, *Journal of Synchrotron Radiation* **21**, 594 (2014).
- [16] T. Beuvier, I. Probert, L. Beaufort, B. Suchéras-Marx, Y. Chushkin, F. Zontone, and A. Gibaud, *Nature Communications* **10**, 751 (2019).
- [17] M. M. Seibert, T. Ekeberg, F. R. N. C. Maia, M. Svenda, J. Andreasson, O. Jonsson, D. Odic, B. Iwan, A. Rocker, D. Westphal, M. Hantke, D. P. DePonte, A. Barty, J. Schulz, L. Gumprecht, N. Coppola, A. Aquila, M. Liang, T. A. White, A. Martin, C. Caleman, S. Stern, C. Abergel, V. Seltzer, J.-M. Claverie, C. Bostedt, J. D. Bozek, S. Boutet, A. A. Miahnahri, M. Messerschmidt, J. Krzywinski, G. Williams, K. O. Hodgson, M. J. Bogan, C. Y. Hampton, R. G. Sierra, D. Starodub, I. Andersson, S. Bajt, M. Barthelmeß, J. C. H. Spence, P. Fromme, U. Weierstall, R. Kirian, M. Hunter, R. B. Doak, S. Marchesini, S. P. Hau-Riege, M. Frank, R. L. Shoeman, L. Lomb, S. W. Epp, R. Hartmann, D. Rolles, A. Rudenko, C. Schmidt, L. Foucar, N. Kimmel, P. Holl, B. Rudek, B. Erk, A. Homke, C. Reich, D. Pietschner, G. Weidenspointner, L. Struder, G. Hauser, H. Gorke, J. Ullrich, I. Schlichting, S. Herrmann, G. Schaller, F. Schopper, H. Soltau, K.-U. Kühnel, R. Andritschke, C.-D. Schroter, F. Krasniqi, M. Bott, S. Schorb, D. Rupp, M. Adolph, T. Gorkhover, H. Hirsemann, G. Potdevin, H. Graafsma, B. Nilsson, H. N. Chapman, and J. Hajdu, *Nature* **470**, 78 (2011).
- [18] J. N. Clark, L. Beitra, G. Xiong, A. Higginbotham, D. M. Fritz, H. T. Lemke, D. Zhu, M. Chollet, G. J. Williams, M. Messerschmidt, B. Abbey, R. J. Harder, A. M. Korsunsky, J. S. Wark, and I. K. Robinson, *Science* **341**, 56 (2013).
- [19] D. Sayre, *Acta Crystallographica* **5**, 843 (1952).
- [20] S. Marchesini, *Review of Scientific Instruments* **78**, 011301 (2007).
- [21] J. R. Fienup, *Applied Optics* **52**, 45 (2013).
- [22] P. Thibault and M. Guizar-Sicairos, *New J. Phys.* **14**, 063004 (2012).
- [23] H. N. Chapman, A. Barty, S. Marchesini, A. Noy, S. P. Hau-Riege, C. Cui, M. R. Howells, R. Rosen, H. He, J. C. H. Spence, U. Weierstall, T. Beetz, C. Jacobsen, and D. Shapiro, *J. Opt. Soc. Am. A* **23**, 1179 (2006).
- [24] T. Latychevskaia, Y. Chushkin, F. Zontone, and H.-W. Fink, *Applied Physics Letters* **107**, 183102 (2015).
- [25] A. J. Devaney and R. Chidlaw, *J. Opt. Soc. Am.* **68**, 1352 (1978).
- [26] T. R. Crimmins and J. R. Fienup, *J. Opt. Soc. Am.* **71**, 1026 (1981).
- [27] R. H. T. Bates, *Optik* **61**, 247 (1982).
- [28] M. Hayes, *IEEE Transactions on Acoustics, Speech, and Signal Processing* **30**, 140 (1982).
- [29] R. Bates, *Computer Vision, Graphics, and Image Processing* **25**, 205 (1984).
- [30] J. H. Seldin and J. R. Fienup, *Journal of the Optical Society of America A* **7**, 412 (1990).
- [31] A. Ulvestad, Y. Nashed, G. Beutier, M. Verdier, S. O. Hruszkewycz, and M. Dupraz, *Scientific Reports* **7**, 9920 (2017).
- [32] T. U. Schüllli and S. J. Leake, *Current Opinion in Solid State and Materials Science* **22**, 188 (2018).
- [33] A. Björling, G. Carbone, F. J. Sarabia, S. Hammarberg, J. M. Feliu, and J. Solla-Gullon, Submitted (2019).
- [34] A. T. Brünger, *Nature* **355**, 472 (1992).
- [35] I. J. Tickle, R. A. Laskowski, and D. S. Moss, *Acta Crystallographica Section D Biological Crystallography* **54**, 547 (1998).
- [36] I. J. Tickle, R. A. Laskowski, and D. S. Moss, *Acta Crystallographica Section D Biological Crystallography* **56**, 442 (2000).
- [37] M. H. Quenouille, *The Annals of Mathematical Statistics* **20**, 355 (1949).
- [38] B. Efron and C. Stein, *The Annals of Statistics* **9**, 586 (1981).
- [39] V. Favre-Nicolin, “PyNX, Python tools for Nanos-structure Xtallography and coherent X-ray imaging, <http://ftp.esrf.fr/pub/scisoft/PyNX/>,” (2010).
- [40] M. Guizar-Sicairos, S. T. Thurman, and J. R. Fienup, *Optics letters* **33**, 156 (2008).